

Interaction of the NH₂ Radical with the Surface of a Water Droplet

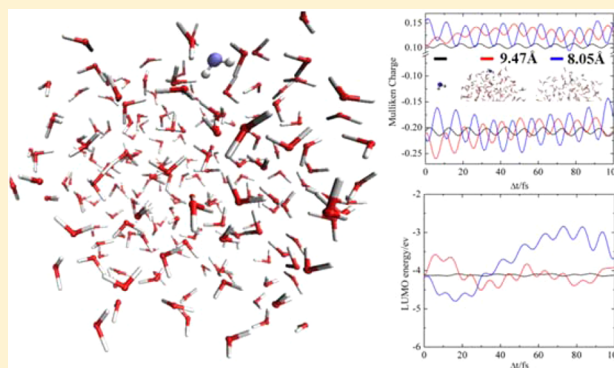
Jie Zhong,[†] Yu Zhao,[†] Lei Li,[†] Hui Li,[‡] Joseph S. Francisco,^{*,†} and Xiao Cheng Zeng^{*,†}

[†]Department of Chemistry, University of Nebraska-Lincoln, Lincoln, Nebraska 68588, United States

[‡]Institute of Physics, Chinese Academy of Sciences, Beijing, 100080, China

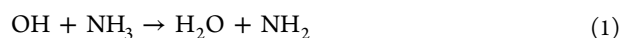
S Supporting Information

ABSTRACT: We present a comprehensive computational study of NH₂ (radical) solvation in a water nanodroplet. The ab initio Born–Oppenheimer molecular dynamics simulation shows that NH₂ tends to accumulate at the air–water interface. The hydrogen-bonding analysis shows that compared to the hydrogen bond of HNH·OH₂, the hydrogen bond of HOH·NH₂ is the dominant interaction between NH₂ and water. Due to the loose hydrogen-bonding network formed between NH₂ and the droplet interface, the NH₂ can easily move around on the droplet surface, which speeds up the dynamics of NH₂ at the air–water interface. Moreover, the structural analysis indicates that the NH₂ prefers an orientation such that both N atom and one of its H atoms interact with the water droplet, while the other H atom is mostly exposed to the air. As a result, the NH₂ radical becomes more accessible for reaction at the water interface. More importantly, the solvation of NH₂ modifies the amplitude of vibration of the N–H bond, thereby affecting the Mulliken charges and electrophilicity of NH₂. As such, reactive properties of the NH₂ are altered by the droplet interface, and this can either speed up reactions or allow other reactions processes to occur in the atmosphere. Hence, the solvation of NH₂ on water droplets, in chemistry of the atmosphere, may not be negligible when considering the effects of clouds.

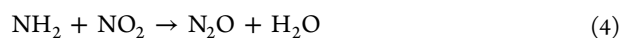


INTRODUCTION

Ammonia in the atmosphere is largely a result of biosphere–atmosphere interactions at the Earth’s surface with emission sources from living organisms, vegetation, and the combustion of biomass.^{1–4} In the atmosphere, NH₃ can be attacked by OH radical and undergo chemical oxidation:



Atmospheric oxidation of NH₃ is a major source of NH₂, which is believed to have significant influence on other N-based trace gases in the troposphere, e.g., NO_x, N₂O, due to the following oxidation reactions:^{5–8}



Because of the important environmental implications for these reactions, they have been extensively investigated using various experimental methods, which allow an assessment of the production or destruction of NO_x or N₂O. Based on previous experimental studies,⁹ the upper limiting reaction rates for the oxidation reactions 2–4 were 0.1 L mol⁻¹ s⁻¹. Such low reaction rates might rule out their atmospheric significance; however, this view needs re-evaluation because most published models on the oxidation of the NH₂ radical assume that the

NH₂ is entirely in the gas phase. Effects of aerosols and clouds have not been considered for the NH₂ radical. In the atmosphere, aerosols and clouds also play crucial roles in atmospheric chemistry. Water on a cloud surface can adsorb or react with small radicals and affect/perturb their concentrations in the atmosphere.^{10,11} One such radical is NH₂ which can be present on water droplets for a long time due to high reaction barrier with water (see Figure S1). Moreover, the solvation structure of the NH₂ radical on cloud droplets may affect the radical’s orientation and reactivity, which can influence reaction processes to a large extent.^{12,13} Lastly, heterogeneous reactions are often involved for radicals in clouds, which might allow otherwise forbidden chemistry to occur in the atmosphere.^{14,15}

As a result, the interaction of NH₂ radicals with water interfaces is important to understand, how oxidation reactions of NH₂ are impacted by the presence of clouds or aerosols in the atmosphere. This has not been addressed for the NH₂ radical.

Few experimental studies on cloud droplet–radical interactions have been reported in the literature due in part to the challenges of measuring radical reactivity and lifetime in water droplets.¹⁶ Recently, molecular dynamics (MD) simulations have been successfully applied to investigate the interaction between important atmospheric species, such as OH, ClO, and HO₂ radicals, and water droplets.^{16–18} These simulation results

Received: July 15, 2015

Published: September 1, 2015

have provided a new picture of the behavior of small radicals at a water droplet interface. As mentioned above, the interaction between NH_2 radical and a cloud droplet is largely unknown nor is the solvation structure of NH_2 in clouds known. In view of the lack of data, the aim of this study is to provide insight into the accommodation behavior, structure characteristic, and electronic properties (hence reactivity) of NH_2 radical at the air–water interface, which may bring new insights into the oxidation of NH_2 at atmosphere. Toward this end, we perform the first ab initio Born–Oppenheimer molecular dynamics (BOMD) simulations at the gradient-corrected density functional theory (DFT) level with inclusion of semiempirical dispersion correction to investigate structural and dynamic properties of an NH_2 radical interacting with a water nanodroplet.

COMPUTATION METHODS

In the BOMD simulation, the water droplet composed of 191 water molecules and 1 NH_2 radical. The dimension of the simulation box is $x = 35 \text{ \AA}$, $y = 35 \text{ \AA}$, $z = 35 \text{ \AA}$, which is large enough to avoid interactions between adjacent periodic images of water droplet. To ensure equilibration of the droplet/ NH_2 system, two very different initial positions for the NH_2 radical are considered. As depicted in Figure 1, NH_2 is initially placed

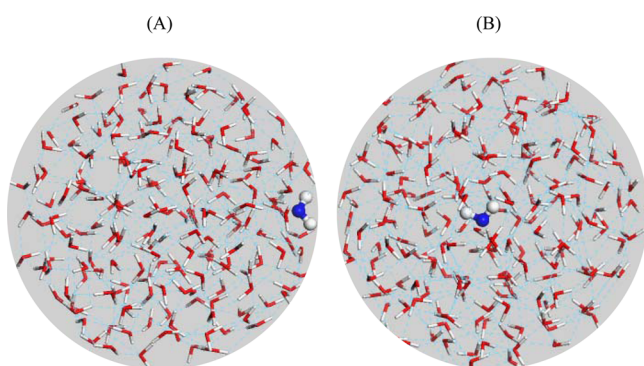


Figure 1. Initial positions of the NH_2 radical in the water droplet: (A) at the surface region ($R_{\text{NH}_2\text{-COM}} \approx 9.5 \text{ \AA}$), (B) in the interior region ($R_{\text{NH}_2\text{-COM}} \approx 0.3 \text{ \AA}$), where $R_{\text{NH}_2\text{-COM}}$ denotes the distance of NH_2 from the COM of the water droplet. The light blue dash lines represent hydrogen bonds. Red: O; white: H; blue: N.

either in the interior region ($R_{\text{NH}_2\text{-COM}} \approx 0.3 \text{ \AA}$) or in the surface region ($R_{\text{NH}_2\text{-COM}} \approx 9.5 \text{ \AA}$), where $R_{\text{NH}_2\text{-COM}}$ denotes the distance of NH_2 from the center of mass (COM) of the water droplet. Prior to the BOMD simulation, each system is fully relaxed using a spin-polarized DFT method to account for the unpaired electron on the NH_2 radical. Specifically, the Becke–Lee–Yang–Parr (BLYP) exchange–correlation functional is selected for the structure relaxation and BOMD simulations. The BLYP functional has been examined by many previous researchers for BOMD simulations, and it gives very reasonable results.^{19–21} A combination of Gaussian DZVP basis set²² and auxiliary plane waves for expanding electron density, together with the Goedecker–Teter–Hutter (GTH) norm-conserved pseudopotentials^{23,24} for treating core electrons, is adopted for the DFT calculations. Grimme’s dispersion correction method^{25,26} is employed to combine with the BLYP functional, which can give overall more accurate properties of liquid water.²⁷

All the BOMD trajectories are generated in the constant volume and constant temperature (NVT) ensemble, with the Nose–Hoover chain method for controlling the temperature of the system. The integration step is set as 1 fs, which has been proven to achieve sufficient energy conservation for the water systems.²⁸ The total simulation times are 147 and 200 ps, respectively, assuring that the NH_2 can reach their equilibrium positions. All BOMD simulations are carried out using the CP2K program.^{29,30}

RESULTS AND DISCUSSION

Surface Preference. Propensity of the radical at the air–water interface can play a key role in its uptake and chemical reactions in clouds.^{11,31–33} We initially speculated that the NH_2 radical might exhibit bulk preference based on the following two factors: (a) The NH_2 radical can act as both as a hydrogen-bond donor and acceptor and (b) NH_2 has a similar size and structure as a water molecule. Both factors may lead to an energetically favorable interaction between NH_2 and a water droplet, thereby resulting in NH_2 uptake into the droplet. Contrary to this speculation, the “out-layer preference” of NH_2 is seen in our BOMD simulations. As shown in Figure 2A, the distance between NH_2 and the COM of water droplet ($R_{\text{NH}_2\text{-COM}}$) is plotted as a function of time. The horizontal dashed line located at 10.5 \AA is defined as the air–water

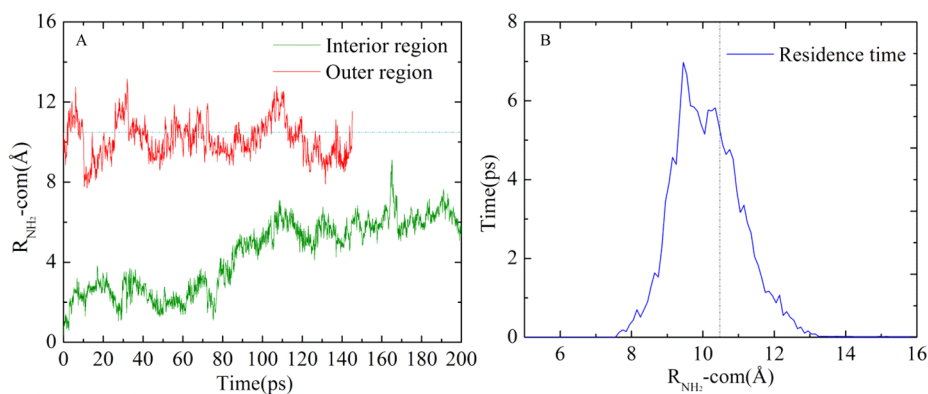


Figure 2. (A) The distance between NH_2 and the COM of water droplet versus the simulation time. Here, the horizontal dashed line located at 10.5 \AA is defined as the air–water interface position. (B) The residence time of NH_2 at different distances between NH_2 and the COM of water droplet. The analysis is based on the BOMD trajectory with NH_2 being initially placed near the surface region.

interface position (see Figure S2 for the reason for this definition). When NH_2 is initially placed in the interior region, the NH_2 appears to be driven gradually toward the air–water interface in the course of the 200 ps BOMD simulation (see Movie S1). When NH_2 is initially placed near the surface region, the NH_2 moves back and forth near the border of the interface. Both simulations indicate an “out-layer preference” for the NH_2 in water nanodroplet. To better understand this “outer-layer preference” behavior, we record the “residence time” of NH_2 at different distances of $R_{\text{NH}_2\text{-COM}}$ in Figure 2B. Here, the resident time is computed (or defined) based on the probability that NH_2 stays at the specific shell (± 0.1 Å from the distance $R_{\text{NH}_2\text{-COM}}$) of the water droplet during the course of simulation. From Figure 2B, one can see that the NH_2 radical shows longer residence time at the surface of water droplet (note the peak is located at about $R_{\text{NH}_2\text{-COM}} \approx 9.5$ Å). In other words, the NH_2 tends to accommodate at the air–water interface.

Radial Distribution Functions for H_2O – H_2O and NH_2 – H_2O . Another structural feature that illustrates the “outer-layer preference” of NH_2 is the radial distribution functions (RDFs) for H_2O – H_2O and NH_2 – H_2O as shown in Figure 3. The unit of RDF used here is arbitrary in the sense that it is a relative unit of measurement to show the relative atom distribution versus the distance between two concerning atoms. For water in the interior region of the droplet, the RDF of $\text{HOH}\cdots\text{OH}_2$ shows the formation of hydrogen bonds among water molecules. Integration of the first peak leads to the hydration numbers of 1.95 (Figure 3B). For NH_2 radical in the interior region of the droplet, the N atom appears to form a relatively weak hydrogen bond with surrounding H atoms in water (see RDF for $\text{HOH}\cdots\text{NH}_2$), which gives a small hydration number of 1.02, about half of that of O (H_2O) in the interior region. The RDF for $\text{HNNH}\cdots\text{OH}_2$ shows that the terminal H atoms in NH_2 form no obvious hydrogen bond with surrounding O atoms (see green curve in Figure 3A and the lowest green bar in Figure 3B).

Figure 4 illustrates a snapshot of BOMD simulation in the early stage, where it shows that the neighboring O and H atoms in different water molecules can form hydrogen bonds with the hydration number being approximate 2 for O atoms (the hydration number for H atoms is half of that of O atoms). However, for NH_2 , the N atom can form a relatively weak hydrogen bond with the surrounding water, and the hydration number is just about 1. As such, the NH_2 radical is not energetically favored to be integrated into the dynamic hydrogen-bonding network formed in the interior region of the droplet. So it is gradually driven to the air–water interface.

For water molecules at the surface, the first peak of the RDF for $\text{HOH}\cdots\text{OH}_2$ is notably lowered, giving a hydration number of 1.37. However, for NH_2 at the surface, the first peak of RDF for $\text{HOH}\cdots\text{NH}_2$ does not show an obvious change compared to that in the interior region of the droplet. The corresponding hydration number is 1.13, close to that (1.37) for $\text{HOH}\cdots\text{OH}_2$ of surface water. As such, the NH_2 radical can be integrated into the looser hydrogen-bonding network in the outer-layer of the droplet, binding with an interfacial H_2O through the hydrogen bond after arriving at the surface ($R_{\text{NH}_2\text{-COM}} > 10.5$ Å).

Next, the detailed adsorption behavior for NH_2 at the air–water interface is analyzed, including the hydrogen-bonding network, conformational dynamics, orientation, and electronic properties of NH_2 radical. Considering the equilibrium position

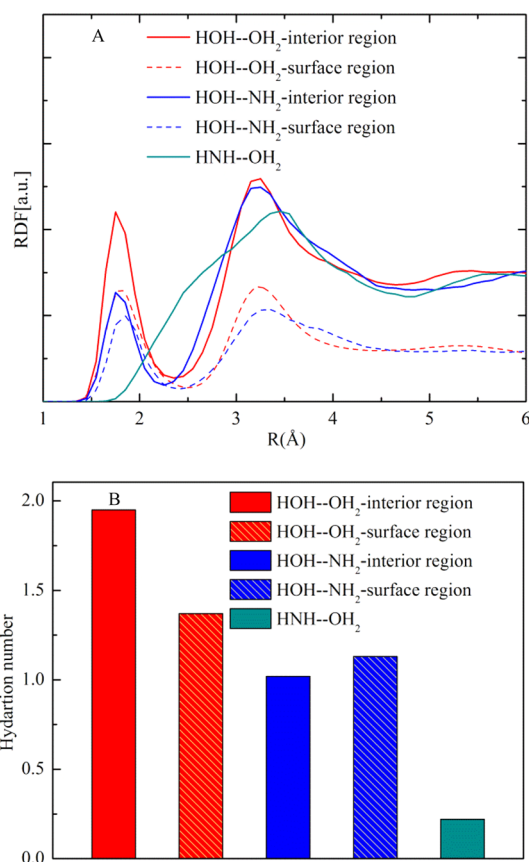


Figure 3. (A) Radical distribution functions (in arbitrary unit) for NH_2 – H_2O and H_2O – H_2O . Red curve represents RDF for $\text{HOH}\cdots\text{OH}_2$ in the interior region of droplet, the dash red curve represents RDF for $\text{HOH}\cdots\text{OH}_2$ in the surface region, the blue curve represents RDF for $\text{HOH}\cdots\text{NH}_2$ in the interior region of droplet, the dash blue curve represents RDF for $\text{HOH}\cdots\text{NH}_2$ in the surface region, and the green curve represents RDF for $\text{HNNH}\cdots\text{OH}_2$. (B) Histograms of hydration number calculated by integrating the first peak of the RDF curves. Colors of histograms correspond to those of relevant RDF curves.

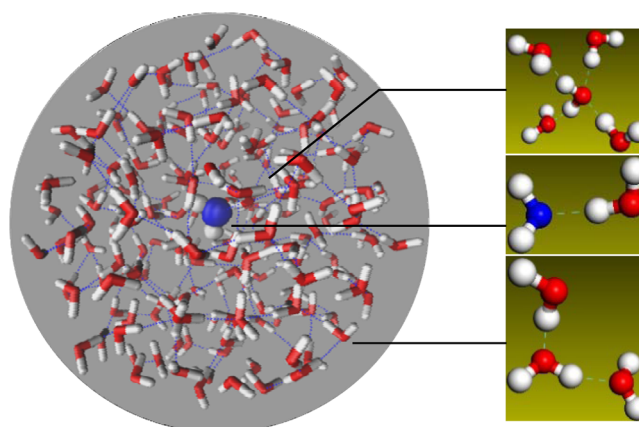


Figure 4. Snapshot at early stage of BOMD shows the NH_2 radical interacts with H_2O (middle); H_2O interacts with H_2O in the interior region (upper) and at the surface (bottom) of the droplet.

of NH_2 being at the air–water interface, the analysis is based on the BOMD trajectory with NH_2 being initially placed near the surface region.

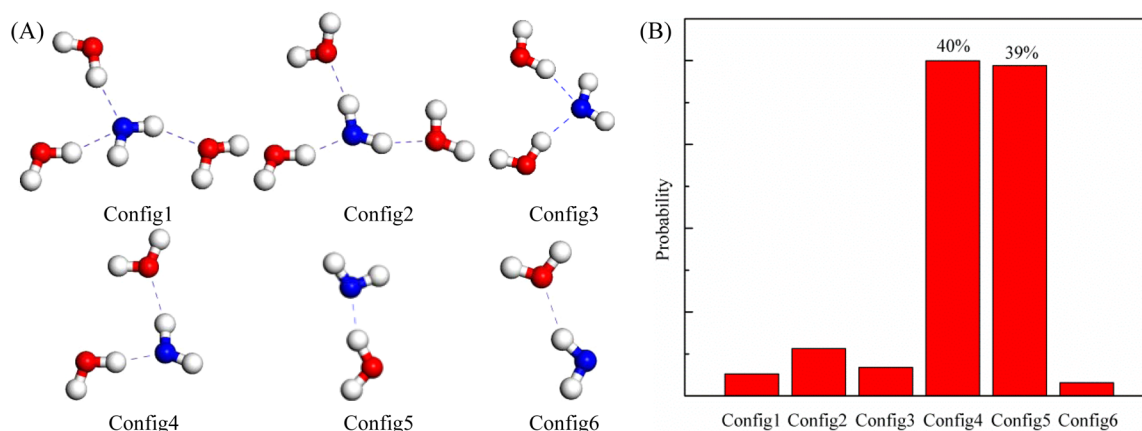


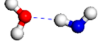
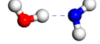
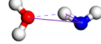
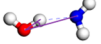
Figure 5. (A) Six typical hydrogen-bonding complexes between $\text{NH}_2\text{-H}_2\text{O}$. Config1 corresponds to 2 $\text{HOH}\cdots\text{NH}_2$ and 1 $\text{HNH}\cdots\text{OH}_2$ hydrogen bonds. Config2 corresponds to 1 $\text{HOH}\cdots\text{NH}_2$ and 2 $\text{HNH}\cdots\text{OH}_2$ hydrogen bonds. Config3 corresponds to 2 $\text{HOH}\cdots\text{NH}_2$ hydrogen bonds. Config4 corresponds to 1 $\text{HOH}\cdots\text{NH}_2$ and 1 $\text{HNH}\cdots\text{OH}_2$. Config5 corresponds to 1 $\text{HOH}\cdots\text{NH}_2$ hydrogen bond. Config6 corresponds to 1 $\text{HNH}\cdots\text{OH}_2$ hydrogen bond. The blue dash lines represent hydrogen bonds. For atom color codes see caption of Figure 1. (B) Histograms of probabilities of different hydrogen-bonding complexes.

Hydrogen-Bonding Network Surrounding NH_2 . The interaction between NH_2 and water droplet is mainly contributed by the hydrogen bonds. First, the average number of hydrogen bonds formed by NH_2 and water droplet is calculated. Our model specified a hydrogen bond between NH_2 and H_2O , if the O–N distance was <3.5 Å and simultaneously the angle N–O··H or O–N··H was $<30^\circ$.³⁴ The calculated average number of hydrogen bonds formed between NH_2 and water is 1.50 at the air–water interface. Among them, 1.00 hydrogen bond is attributed by the hydrogen bond of $\text{HOH}\cdots\text{NH}_2$, whereas only 0.50 hydrogen bond is attributed by the hydrogen bond of $\text{HNH}\cdots\text{OH}_2$. This result implies that the N atom can form more hydrogen bonds with water droplet than that of the two H atoms in NH_2 , which is consistent with previous RDF analysis.

To gain deeper understanding of the hydrogen-bonding network surrounding NH_2 radical, six typical hydrogen-bonding complexes are considered as shown in Figure 5A. (Definition for the six hydrogen-bonding complexes is given in the caption.) The histogram of Figure 5B shows the probabilities of these complexes. It can be seen that Config4 and Config5 exhibit the highest probability, which accounts for nearly 80% of all complexes. These results indicate that the N atom tends to form one hydrogen bond with surrounding H atoms during all the simulation time. And for the two H atoms in NH_2 , there are two different situations. In about half of the simulation time, one of the two H atoms can form a hydrogen bond with the surrounding O atoms. In the remaining simulation time, no hydrogen bond is formed by any of the H atoms in NH_2 . Meanwhile, it can be seen that the probabilities of Config1 and Config2 are very small, which means the $\text{NH}_2\text{-water}$ can hardly form dense hydrogen-bonding networks.

To evaluate the strength of the hydrogen bonds of $\text{HOH}\cdots\text{NH}_2$ and $\text{HNH}\cdots\text{OH}_2$, the corresponding structural parameters (e.g., H··O, H··N bond lengths and N–O··H, O–N··H angles) of all six complexes are calculated (see Table 1). First, one can see that the average bond length of $\text{HOH}\cdots\text{NH}_2$ is much smaller than that of $\text{HNH}\cdots\text{OH}_2$ in nearly all the complexes. Even for Config1 and Config3 where two hydrogen bonds of $\text{HOH}\cdots\text{NH}_2$ are formed with the N atom at the same time, the bond length of $\text{HOH}\cdots\text{NH}_2$ is still shorter than that of the $\text{HNH}\cdots\text{OH}_2$. Meanwhile, the angle of O–N··H is much

Table 1. A Summary of Computed Geometry Parameter (H··O, H··N Bond Lengths and O–N··H, N–O··H Angles) of Six Complexes

				
	length (Å)	length (Å)	angle(°)	angle(°)
Config1	2.23	2.11	19.21	16.54
Config2	2.26	1.86	18.31	11.77
Config3		2.10		15.24
Config4	2.21	1.89	18.02	12.58
Config5		1.93		12.86
Config6	2.26		19.69	

larger than that of N–O··H. Both results indicate that the hydrogen bond of $\text{HOH}\cdots\text{NH}_2$ is much stronger than that of $\text{HNH}\cdots\text{OH}_2$. The strength of the hydrogen bonds can also be verified by the interaction energy between NH_2 and water in Config5 and Config6. We use the MP2/6-31+G(d,p) level of theory implemented in Gaussian 09 package³⁵ to optimize both structures. The counterpoise method is used in computing the binding energy to account for the basis set superposition errors (BSSEs) for the hydrogen-bonded systems. The computed interaction energy of Config5 is 4.93 kcal/mol which is much greater than that of Config6 (2.84 kcal/mol). This result also confirms the findings from the BOMD simulations.

Next, we study the dynamic stability of the hydrogen bonds between NH_2 and water by computing the correlation function $C(t)$. The correlation function $C(t)$ of the hydrogen bond lifetime for $\text{HOH}\cdots\text{NH}_2$, $\text{HNH}\cdots\text{OH}_2$ is given by³⁶

$$\langle C(t) \rangle = \left\langle \frac{1}{N_{S1}} \sum_{i=1}^{N_{S1}} [h_i(0)h_i(t)] \right\rangle \quad (1)$$

where N_{S1} is the hydrogen bond number, $h_i(t)$ is 1 or 0 for a hydrogen bond formed or broken at time t .

Computed $C(t)$ (Figure 6) shows that the decay rate of the correlation function of the lifetime for $\text{HOH}\cdots\text{NH}_2$ is much

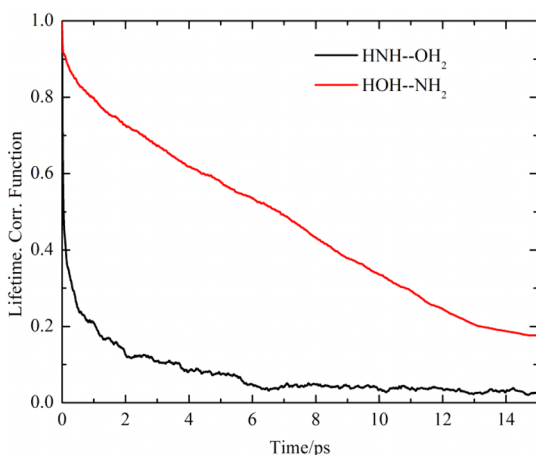


Figure 6. Correlation function of the hydrogen-bond lifetime for $\text{HOH}\cdots\text{NH}_2$ and $\text{HNH}\cdots\text{OH}_2$.

slower than that of $\text{HNH}\cdots\text{OH}_2$. It indicates that the hydrogen bond of $\text{HOH}\cdots\text{NH}_2$ is more stable due to the stronger hydrogen-bonding interaction. In summary, the average

number, strength, and lifetime of the hydrogen bonds show that the interaction between NH_2 and water is dominated by the $\text{HOH}\cdots\text{NH}_2$ interaction.

Orientation of Water in the First Hydrated Shell Around NH_2 . The orientation of a water molecule relative to the NH_2 can be uniquely defined by two angular coordinates, θ_μ and φ .^{37,38} The θ_μ is the angle formed by the vector between the water oxygen and the center of the NH_2 radical \vec{r}_{ON} , and the dipole moment vector of the water molecule $\vec{\mu}$, where \vec{r}_{ON} points in the direction of the NH_2 . The coordinate φ is the angle made by the projection of \vec{r}_{ON} onto a local XY -plane and the local X -axis which is normal to the $\text{H}-\text{O}-\text{H}$ plane.

First, the radius of the first hydrated shell around NH_2 is confirmed by radial distribution function (RDF) between NH_2 and H_2O (see Figure S3). Next, joint probability distributions $P(\theta_\mu, \varphi)$ for water molecules within the first hydration shell are computed and depicted in Figure 7A,B (NH_2 in the surface and interior regions, respectively). For comparison, the joint probability distribution $P(\theta_\mu, \varphi)$ for water molecules around a H_2O is also computed using the same method (see Figure 7C). Based on the computed $P(\theta_\mu, \varphi)$, the sketches for the orientation between NH_2 and H_2O , H_2O and H_2O in the high probability region are depicted in Figure 7D–F, respectively.

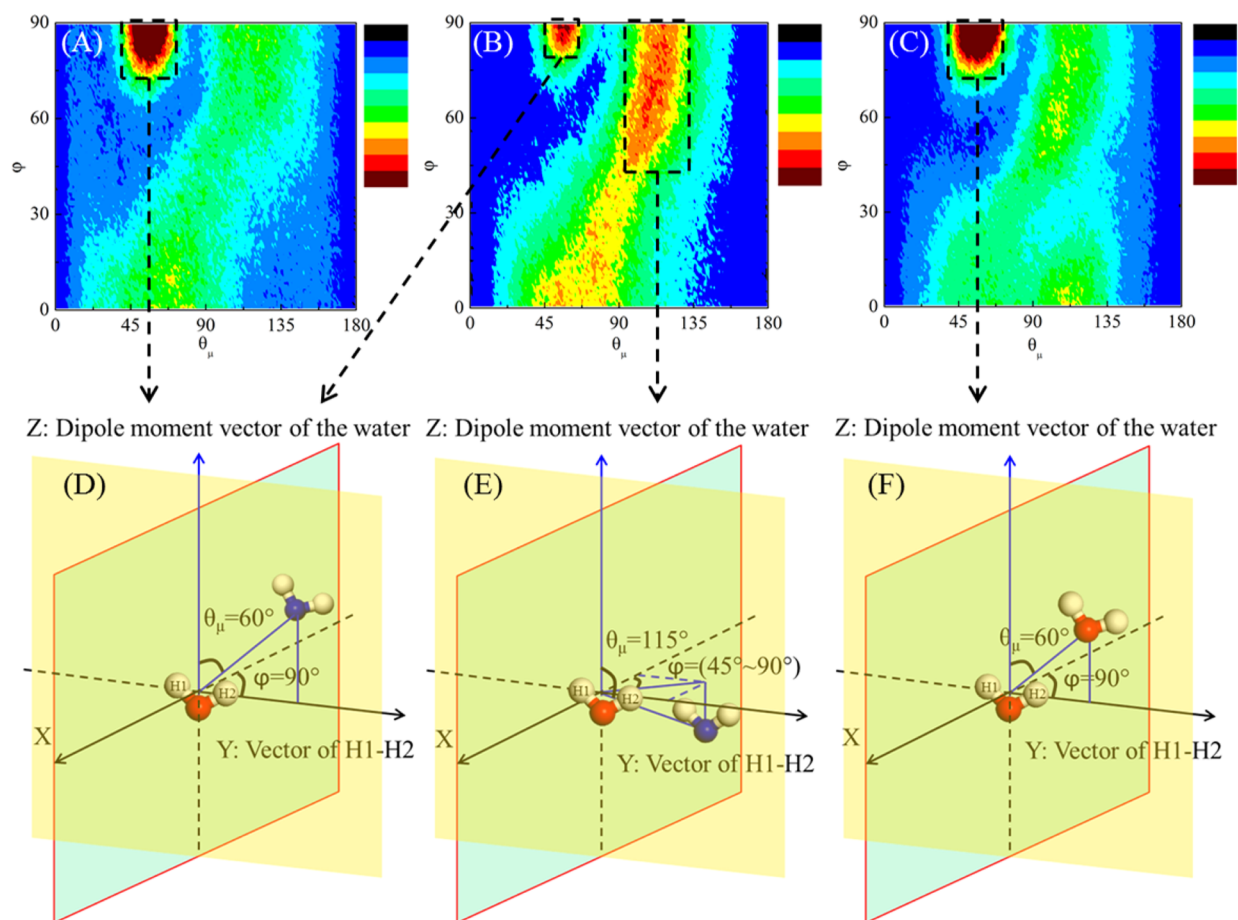


Figure 7. Joint probability distributions $P(\theta_\mu, \varphi)$ computed for water molecules within the first hydration shell of the NH_2 radical are depicted in (A) for NH_2 in the surface region and in (B) for NH_2 in the interior region, respectively, and that around a H_2O molecular is depicted in (C). Red denotes high probability, while blue denotes low probability. The sketches for the orientation between NH_2 and H_2O , H_2O and H_2O in the high probability region are depicted in (D, E, and F).

For NH_2 at the surface, the dominant orientation (Figure 7D) is such that both NH_2 and H_2O are in the YZ plane due to the hydrogen bond of $\text{HOH}\cdot\text{NH}_2$. It indicates that the interaction between NH_2 and water droplet at the surface is mainly contributed by the hydrogen bond of $\text{HOH}\cdot\text{NH}_2$, consistent with the analysis in the Hydrogen-Bonding Network Surrounding NH_2 section. The orientation between H_2O and H_2O depicted in Figure 7F is similar to that shown in Figure 7D. Such an orientation is preferred due to the hydrogen-bond formation between water molecules. Unlike the orientation of $\text{H}_2\text{O}-\text{H}_2\text{O}$ or $\text{H}_2\text{O}-\text{NH}_2$ at the surface, there exist two dominant orientations for NH_2 in the interior of the water droplet (see the sketches in Figure 7D,E). Figure 7E shows a relatively large θ_μ due to the hydrogen bond of $\text{HNH}\cdot\text{OH}_2$. Interestingly, the angle φ in Figure 7E is found to have a relatively wide angle range from 45° to 90° . This feature suggests that the hydrogen bond of $\text{HNH}\cdot\text{OH}_2$ is less stable in the water droplet, which may be viewed as a type of hydrogen-bond defect. This hydrogen-bonding defect may give an explanation for the NH_2 migration from the interior of the water droplet to the air–water interface.

Diffusion Coefficients of NH_2 . First, the dynamic property of NH_2 at the air–water interface is computed. The diffusion constant (D) can be evaluated from the mean square displacement (Figures S4 and S5) using the Einstein's diffusion equation:³⁹

$$|r(t) - r(0)|^2 = 6Dt \quad (2)$$

As shown in Table 2, the computed diffusion constant of the radical NH_2 is $1.57 \times 10^{-5} \text{ cm}^2/\text{s}$, larger than the self-diffusion

Table 2. Diffusion Coefficient (D) of NH_2 in the Outer-Layer of the Water Droplet

	NH_2 -total	NH_2 -radial	NH_2 -angular
D ($10^{-5} \text{ cm}^2/\text{s}$)	1.57	1.47	0.10

constant of water molecules in the interior region ($D_w = 6 \times 10^{-6} \text{ cm}^2/\text{s}$). This result indicates that the NH_2 exhibits relatively high mobility at the water–air interface. On the other hand, when the NH_2 is initially placed near the surface region, the NH_2 radical exhibits oscillatory movement at the water–air interface during the simulation, implying low mobility. To

reconcile the apparent contradiction, we decompose the diffusion constant of the NH_2 into two terms: one due to angular motion and another due to radial motion. It can be seen that diffusion of NH_2 in the radial direction is indeed very small and even can be neglected compared with the angular diffusion. So the larger diffusion constant of NH_2 is mainly due to motion in the angular direction. This is consistent with the previous finding, i.e., NH_2 only forms a loose hydrogen-bonding network.

Orientation of NH_2 . Next, preferred orientation of NH_2 at the outer-layer of droplet is analyzed. Three typical configurations (I, II, and III) are shown in Figure 8A (definitions for the three configurations I, II, and III are given in the caption). Because the orientation of the NH_2 is largely affected by the surrounding water molecules, it constantly changes as the NH_2 moves back and forth crossing the boundary of the air–water interface. In Figure 8B, we plot the probability of configurations I, II, and III versus $R_{\text{NH}_2-\text{COM}}$. It can be seen that in the whole range of $R_{\text{NH}_2-\text{COM}}$, configuration III has the highest probability, indicating that the N atom tends to be located such that its distance from the COM of the water droplet $R_{\text{N-com}}$ is between $R_{\text{H1-com}}$ and $R_{\text{H2-com}}$. Moreover, the probability of configuration I increases gradually as $R_{\text{NH}_2-\text{COM}}$ becomes larger, suggesting that as NH_2 migrates to the surface, the N atom tends to be closer to the COM than the other two H atoms. This feature can be ascribed to the hydrogen-bond formation between N (NH_2) with H (H_2O). When the NH_2 is at the surface, the configuration I allows the N (NH_2) and H (H_2O) to form hydrogen bonds more easily.

Although configuration I is favorable for hydrogen bond formation $\text{HOH}\cdot\text{NH}_2$ at large $R_{\text{NH}_2-\text{COM}}$, one may ask why the probability of configuration III is higher than that of configuration I. To address this question, the microstructure of configuration III should be analyzed in more detail because configuration III is energetically favorable for the coulomb interaction between H1 (NH_2) (the H atom with shorter distance to COM of droplet) and O (H_2O). To evaluate the microstructure for configuration III, the average angles of θ_1 and θ_2 as shown in the inset of Figure 9A are computed as a function of $R_{\text{NH}_2-\text{COM}}$. It can be seen that θ_2 is about 5° for all

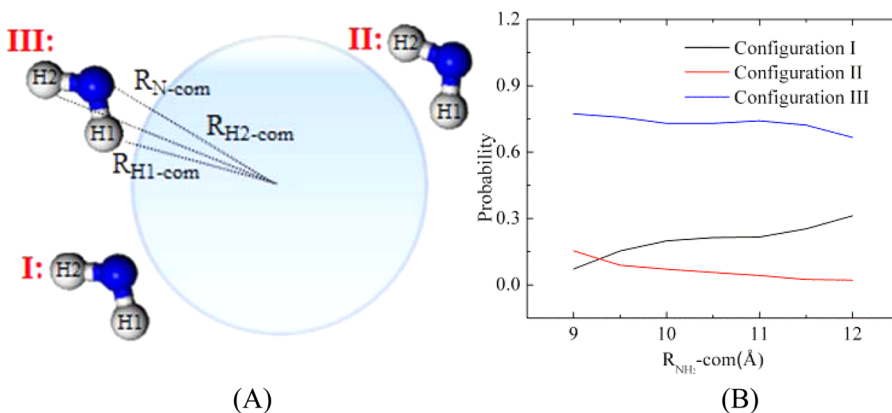


Figure 8. (A) Definition of configuration I, II and III. $R_{\text{N-com}}$, $R_{\text{H1-com}}$ and $R_{\text{H2-com}}$ represent the distance between N (NH_2), H1 (NH_2), and H2 (NH_2) with COM of water droplet, respectively. (H1 is the hydrogen atom in NH_2 with shorter distance to the COM of water droplet). Configuration I corresponds to $R_{\text{N-com}} < R_{\text{H1-com}} < R_{\text{H2-com}}$. Configuration II corresponds to $R_{\text{N-com}} > R_{\text{H2-com}} > R_{\text{H1-com}}$. Configuration III corresponds to $R_{\text{H1-com}} < R_{\text{N-com}} < R_{\text{H2-com}}$. (B) The probability for configurations I, II, III versus the distance between NH_2 and COM of the water droplet.

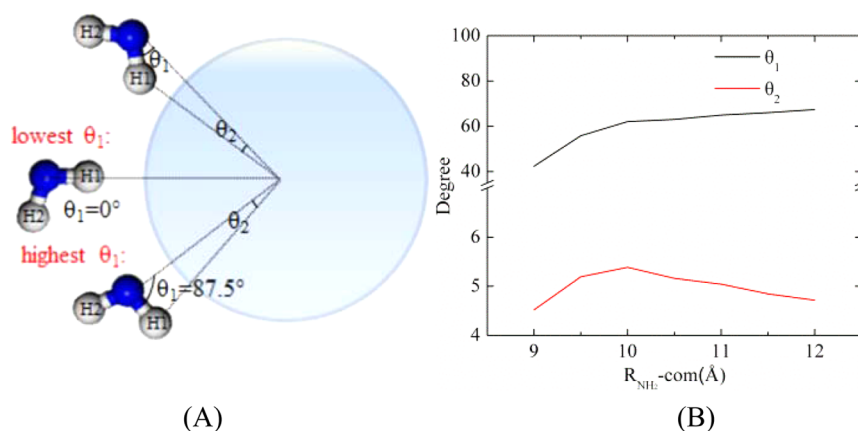


Figure 9. (A) Definition of θ_1 and θ_2 . θ_1 is the angle between the N–H1 bond and N...COM line. θ_2 is the angle between N...COM line and H1...COM line. The lowest θ_1 corresponds to the configuration such that N–H1 bond is parallel to N–COM line ($\theta_1 = 0^\circ$). The highest θ_1 corresponds to the configuration such that $R_{\text{N-COM}} = R_{\text{H1-COM}}$ ($\theta_1 = 87.5^\circ$). (B) The average value of θ_1 and θ_2 versus the distance between NH_2 and COM of water droplet.

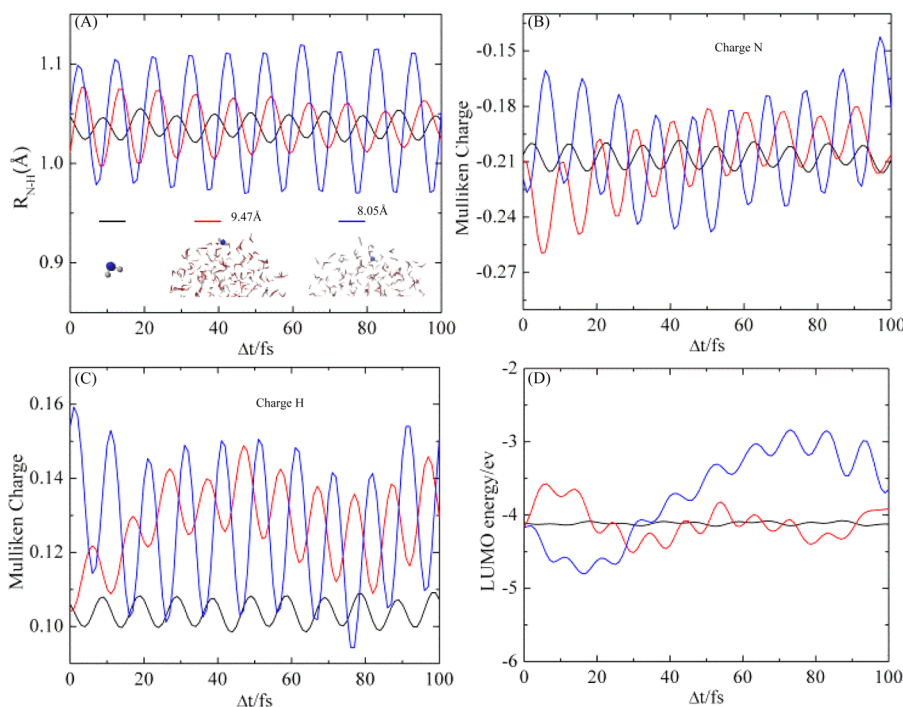


Figure 10. Time evolution of (A) the length of N–H bond, (B) Mulliken charge of N in NH_2 , (C) Mulliken charge of an H in NH_2 , and (D) LUMO energy of NH_2 , within a very short period (100 fs) for a gas-phase NH_2 radical and for NH_2 in the water droplet. The black curve represents the NH_2 in the gas phase; the red and blue curves represent the NH_2 at the air–water interface with the distance between NH_2 and the COM of water droplet being about 9.47 and 8.05 Å, respectively (see insets in (A)). The initial time t_0 is arbitrary.

$R_{\text{NH}_2\text{-COM}}$. Approximating θ_2 as a constant of 5° , the angle of θ_1 should be in the range from 0° to 87.5° (see Figure 9A). If the microstructure for configuration III does not have a preferred direction, the expected average value for θ_1 should be approximately 43.75° . However, only when the $R_{\text{NH}_2\text{-COM}}$ is small enough, θ_1 is close to the expected value. As $R_{\text{NH}_2\text{-COM}}$ increases, θ_1 becomes larger. This result indicates that as NH_2 moves to the air–water interface, the H1 atom keeps moving away from the droplet. This allows the N atom to form a hydrogen bond with water more easily. Above analysis indicates the interaction between NH_2 with H_2O is mainly contributed by the hydrogen bond of $\text{HOH}\cdots\text{NH}_2$. Adjusting the configuration III with large θ_1 (nearly 70° at large distance

of $\text{NH}_2\text{-COM}$) can still retain the dominant hydrogen-bond interaction between N (NH_2) with H (H_2O), while minimizing the coulomb potential for H1 (NH_2) with O (H_2O) to some extent. The angle distribution of θ_1 and θ_2 at different $R_{\text{NH}_2\text{-COM}}$ (see Figure S6) also indicates that the θ_1 tends to distribute at larger angle as NH_2 moves to the outside, while the distribution of the θ_2 almost keeps constant. Overall, the simulation results indicate that the most probable configuration for NH_2 radical at the air–water interface is when the NH_2 interacts with surface water via both the terminal H1 atom and N atom. Such an orientation of NH_2 on the surface suggests the H2 (the H atom with longer distance to the COM of the water droplet) of NH_2 tends to be exposed outward. As a result, the

NH₂ radical becomes more accessible for reaction at the surface.

Vibration of NH₂. Vibration of the N–H bond can affect the coulomb interaction and chemical reactivity. Figure 10A compares the amplitude of vibration of the N–H bond in the gas phase and at the air–water interface. It can be seen that in the gas phase, the amplitude of the N–H bond vibration is much smaller compared to that at the air–water interface. Comparing the amplitude of vibration of the N–H bond at different $R_{\text{NH}_2-\text{com}}$, it appears that the vibration becomes stronger as NH₂ moves to the interior region of water droplet. The vibrational spectra of NH₂ are computed via the Fourier transformation of the velocity autocorrelation function (see Figure S7). For NH₂ in the gas phase, the spectrum exhibits three vibrational peaks at 1515, 3327, and 3413 cm⁻¹, respectively, corresponding to the H–N–H angle bending, symmetric and asymmetric N–H stretching modes, respectively. For NH₂ in the droplet, the positions of the three peaks are not significantly changed from those in the gas phase. This is reasonable as NH₂ radical cannot form strong hydrogen bonds with the water droplet.

Atomic Charges of NH₂. The atomic charges for NH₂ (N: -0.236, H: 0.118) are very small. As a result, it can be hardly polarized by water. Figure 10B,C depicts time evolution of the Mulliken charge of N and an H atom in NH₂ radical. Clearly, the magnitude of Mulliken charge exhibits a similar trend as that of the N–H bond. In the water droplet, the N and H atoms can carry more charges in some periods. This implies that other radicals with opposite charges in the atmosphere would be attracted more strongly by NH₂ in the droplet, thereby increasing their collision probability for reaction. Because the Mulliken charges can be basis-set dependent, the natural charges are also computed, using the natural bond orbital analyses,³⁵ to verify the charge oscillation behavior (see Figure S8).

Solvation effects on the chemical properties of the NH₂ radical can be analyzed via the highest occupied and lowest unoccupied molecular orbitals, HOMO and LUMO. As seen from the electron distribution with frontier orbitals (Figure S9), the HOMO is contributed by the water molecules, whereas LUMO is contributed by the NH₂ radical. The latter indicates NH₂ is electrophilic, which would be attacked by nucleophilic species in the atmosphere. The solvation effects on electrophilicity of NH₂ can be seen from Figure 10D where the LUMO frontier orbital energies of NH₂ in the gas phase and at the air–water interface are compared. Unlike the oscillation of the N–H bond and Mulliken charge, the oscillation of frontier orbital energies is not strictly periodic. Again, however, the amplitude of the oscillation becomes larger for NH₂ in the water droplet. The LUMO energies of NH₂ at air–water interface can be 0.71 eV lower than that in the gas phase. [Calculated LUMO energy vibration at different Δt and $R_{\text{NH}_2-\text{com}}$ (see Figure S10) also shows the same tendency.] Such large decrease of the LUMO energy suggests significant enhancement of electrophilicity for NH₂ radical, which can either speed up the reaction with nucleophilic species or allow other kinetically unfavorable processes to occur in the atmosphere.

CONCLUSIONS

In conclusion, properties of NH₂, one of most abundant radicals in the atmosphere, are studied using BOMD

simulations. The results show that NH₂ tends to be at the air–water interface. Hydrogen-bonding network analysis shows that compared to the hydrogen bond of HNH₂·OH₂, the hydrogen bond of HOH·NH₂ is the dominant interaction between NH₂ and water. Due to the loose hydrogen-bonding network formed between NH₂ with water droplet, the NH₂ can easily move around at the droplet surface, which can speed up dynamics of NH₂ at the air–water interface. Structural analysis indicates that the most probable orientation for the NH₂ radical at air–water interface is the configuration III with the NH₂ interacting with droplet via both N atom and its H atom. As such, the other H atom of NH₂ is mostly exposed to the air, and the NH₂ radical becomes more accessible for reaction at the water surface. More importantly, the solvation of NH₂ modifies the amplitude of vibration of the N–H bond, thereby strongly affecting the Mulliken charges and electrophilicity of NH₂. Compared to NH₂ in the gas phase, the NH₂ at the droplet surface can carry more Mulliken charge and become more electrophilic. Such a change in electronic properties will impact the reactivity of the NH₂ radical in the atmosphere. In other words, the solvation effect for NH₂ cannot be neglected in the chemistry in atmosphere and hence cannot be ignored in atmospheric models of chemistry in the atmosphere, especially when considering cloud effects.

ASSOCIATED CONTENT

Supporting Information

The Supporting Information is available free of charge on the ACS Publications website at DOI: 10.1021/jacs.5b07354.

Definition of the location of air–water interface, the curves of the means square displacement versus time, the angle distribution at different $R_{\text{NH}_2-\text{com}}$, LUMO frontier orbital energies vibration at different $R_{\text{NH}_2-\text{com}}$ are collected (PDF)

Movie of NH₂ in a water droplet (MPG)

AUTHOR INFORMATION

Corresponding Authors

*xzeng1@unl.edu

*jfrancisco3@unl.edu

Notes

The authors declare no competing financial interest.

ACKNOWLEDGMENTS

We thank Profs. Rongxing He and Jaeil Bai and Drs. Jun Wang and Chongqin Zhu for valuable discussions. This work is supported by the National Science Foundation (CHE-1500217) and by the University of Nebraska Holland Computing Centre.

REFERENCES

- (1) Behera, S.; Sharma, M.; Aneja, V.; Balasubramanian, R. *Environ. Sci. Pollut. Res.* **2013**, *20*, 8092.
- (2) Katata, G.; Hayashi, K.; Ono, K.; Nagai, H.; Miyata, A.; Mano, M. *Agricultural and Forest Meteorology* **2013**, *180*, 1.
- (3) Kruit, R. W.; Schaap, M.; Sauter, F. J.; van Zanten, M. C.; van Pul, W. A. J. In *Air Pollution Modeling and its Application XXII*; Steyn, D. G., Builtjes, P. J. H., Timmermans, R. M. A., Eds.; Springer: Netherlands, 2014, 309.
- (4) Wichink Kruit, R. J.; Schaap, M.; Sauter, F. J.; van Zanten, M. C.; van Pul, W. A. J. *Biogeosciences* **2012**, *9*, 5261.

- (5) Jung, M.-Y.; Well, R.; Min, D.; Gieseemann, A.; Park, S.-J.; Kim, J.-G.; Kim, S.-J.; Rhee, S.-K. *ISME J.* **2014**, *8*, 1115.
- (6) Ngugi, D. K.; Brune, A. *Environ. Microbiol.* **2012**, *14*, 860.
- (7) Patrick, R.; Golden, D. M. *J. Phys. Chem.* **1984**, *88*, 491.
- (8) Zhu, X.; Burger, M.; Doane, T. A.; Horwath, W. R. *Proc. Natl. Acad. Sci. U. S. A.* **2013**, *110*, 6328.
- (9) Tyndall, G. S.; Orlando, J. J.; Nickerson, K. E.; Cantrell, C. A.; Calvert, J. G. *J. Geophys. Res.* **1991**, *96*, 20761.
- (10) Huijnen, V.; Williams, J. E.; Flemming, J. *Atmos. Chem. Phys. Discuss.* **2014**, *14*, 8575.
- (11) Whalley, L. K.; Stone, D.; George, I. J.; Mertes, S.; van Pinxteren, D.; Tilgner, A.; Herrmann, H.; Evans, M. J.; Heard, D. E. *Atmos. Chem. Phys.* **2015**, *15*, 3289.
- (12) Buszek, R. J.; Barker, J. R.; Francisco, J. S. *J. Phys. Chem. A* **2012**, *116*, 4712.
- (13) Vieceli, J.; Roeselová, M.; Potter, N.; Dang, L. X.; Garrett, B. C.; Tobias, D. J. *J. Phys. Chem. B* **2005**, *109*, 15876.
- (14) Guo, J.; Tilgner, A.; Yeung, C.; Wang, Z.; Louie, P. K. K.; Luk, C. W. Y.; Xu, Z.; Yuan, C.; Gao, Y.; Poon, S.; Herrmann, H.; Lee, S.; Lam, K. S.; Wang, T. *Environ. Sci. Technol.* **2014**, *48*, 1443.
- (15) Lou, S.; Liao, H.; Zhu, B. *Atmos. Environ.* **2014**, *85*, 123.
- (16) Codorniu-Hernández, E.; Kusalik, P. G. *J. Am. Chem. Soc.* **2012**, *134*, 532.
- (17) Du, S.; Francisco, J. S.; Schenter, G. K.; Garrett, B. C. *J. Am. Chem. Soc.* **2009**, *131*, 14778.
- (18) Martins-Costa, M. T. C.; Anglada, J. M.; Francisco, J. S.; Ruiz-Lopez, M. F. *Angew. Chem., Int. Ed.* **2012**, *51*, 5413.
- (19) Becke, A. D. *Phys. Rev. A: At., Mol., Opt. Phys.* **1988**, *38*, 3098.
- (20) Lee, C.; Yang, W.; Parr, R. G. *Phys. Rev. B: Condens. Matter Mater. Phys.* **1988**, *37*, 785.
- (21) Zhao, Y.; Li, H.; Zeng, X. C. *J. Am. Chem. Soc.* **2013**, *135*, 15549.
- (22) VandeVondele, J.; Hutter, J. *J. Chem. Phys.* **2007**, *127*, 114105.
- (23) Goedecker, S.; Teter, M.; Hutter, J. *Phys. Rev. B: Condens. Matter Mater. Phys.* **1996**, *54*, 1703.
- (24) Hartwigsen, C.; Goedecker, S.; Hutter, J. *Phys. Rev. B: Condens. Matter Mater. Phys.* **1998**, *58*, 3641.
- (25) Grimme, S. *J. Comput. Chem.* **2004**, *25*, 1463.
- (26) Grimme, S. *J. Comput. Chem.* **2006**, *27*, 1787.
- (27) Baer, M. D.; Mundy, C. J.; McGrath, M. J.; Kuo, I.-F. W.; Siepmann, J. I.; Tobias, D. J. *J. Chem. Phys.* **2011**, *135*, 124712.
- (28) Mareš, J.; Liimatainen, H.; Laasonen, K.; Vaara, J. *J. Chem. Theory Comput.* **2011**, *7*, 2937.
- (29) Lippert, B. G.; Parrinello, J. H.; Michele. *Mol. Phys.* **1997**, *92*, 477.
- (30) VandeVondele, J.; Krack, M.; Mohamed, F.; Parrinello, M.; Chassaing, T.; Hutter, J. *Comput. Phys. Commun.* **2005**, *167*, 103.
- (31) Lim, Y. B.; Tan, Y.; Perri, M. J.; Seitzinger, S. P.; Turpin, B. J. *Atmos. Chem. Phys.* **2010**, *10*, 10521.
- (32) Roeselová, M.; Vieceli, J.; Dang, L. X.; Garrett, B. C.; Tobias, D. J. *J. Am. Chem. Soc.* **2004**, *126*, 16308.
- (33) Shannon, R. J.; Blitz, M. A.; Goddard, A.; Heard, D. E. *Nat. Chem.* **2013**, *5*, 745.
- (34) Wang, C.; Lu, H.; Wang, Z.; Xiu, P.; Zhou, B.; Zuo, G.; Wan, R.; Hu, J.; Fang, H. *Phys. Rev. Lett.* **2009**, *103*, 137801.
- (35) Frisch, M. J.; Trucks, G. W.; Schlegel, H. B.; Scuseria, G. E.; Robb, M. A.; Cheeseman, J. R.; Scalmani, G.; Barone, V.; Mennucci, B.; Petersson, G. A.; Nakatsuji, H.; Caricato, M.; Li, X.; Hratchian, H. P.; Izmaylov, A. F.; Bloino, J.; Zheng, G.; Sonnenberg, J. L.; Hada, M.; Ehara, M.; Toyota, K.; Fukuda, R.; Hasegawa, J.; Ishida, M.; Nakajima, T.; Honda, Y.; Kitao, O.; Nakai, H.; Vreven, T.; Montgomery, J. A., Jr.; Peralta, J. E.; Ogliaro, F.; Bearpark, M.; Heyd, J. J.; Brothers, E.; Kudin, K. N.; Staroverov, V. N.; Kobayashi, R.; Normand, J.; Raghavachari, K.; Rendell, A.; Burant, J. C.; Iyengar, S. S.; Tomasi, J.; Cossi, M.; Rega, N.; Millam, J. M.; Klene, M.; Knox, J. E.; Cross, J. B.; Bakken, V.; Adamo, C.; Jaramillo, J.; Gomperts, R.; Stratmann, R. E.; Yazyev, O.; Austin, A. J.; Cammi, R.; Pomelli, C.; Ochterski, J. W.; Martin, R. L.; Morokuma, K.; Zakrzewski, V. G.; Voth, G. A.; Salvador, P.; Dannenberg, J. J.; Dapprich, S.; Daniels, A. D.; Farkas, Ö.; Foresman, J. B.; Ortiz, J. V.; Cioslowski, J.; Fox, D. J. *Gaussian 09*, Revision D.01; Gaussian, Inc.: Wallingford, CT, 2009.
- (36) Zhu, C.; Li, H.; Huang, Y.; Zeng, X. C.; Meng, S. *Phys. Rev. Lett.* **2013**, *110*, 126101.
- (37) Jedlovszky, P. I.; Vincze, A. r. d.; Horvai, G. *J. Chem. Phys.* **2002**, *117*, 2271.
- (38) Remsing, R. C.; Baer, M. D.; Schenter, G. K.; Mundy, C. J.; Weeks, J. D. *J. Phys. Chem. Lett.* **2014**, *5*, 2767.
- (39) Zhong, J.; Wang, P.; Zhang, Y.; Yan, Y.; Hu, S.; Zhang, J. *Energy* **2013**, *59*, 295.